Complete Heme Proton Hyperfine Resonance Assignments of the *Glycera dibranchiata* Component IV Metcyano Monomer Hemoglobin†

Steve L. Alam‡ and James D. Satterlee*,§

Departments of Biochemistry and Biophysics, and Chemistry, Washington State University, Pullman, Washington 99164-4630

Received November 8, 1993; Revised Manuscript Received January 28, 1994®

ABSTRACT: Monomer hemoglobin component IV is one of three major myoglobin-like proteins found in the erythrocytes of the marine annelid *Glycera dibranchiata.* Unlike myoglobin, all three of these monomer hemoglobin components lack the distal histidine, which is replaced by leucine. This substitution alters the protein's functional properties due to its proximity to the heme ligand binding site. As the initial step toward a full NMR characterization of this protein, a complete set of self-consistent proton NMR assignments for the heme and the proximal histidine of the paramagnetic, metcyano form of native component IV (metGMH4CN) is presented. These assignments relied upon a combination of one- and two-dimensional NMR spectroscopy, including nonselective spin–lattice relaxation time measurements. The metcyano form has been chosen for several reasons: (1) The heme paramagnetism acts as an intrinsic shift reagent which aids in making individual resonance assignments for the heme and neighboring amino acids in the protein's ligand binding site. (2) Heme paramagnetism also enhances proton nuclear relaxation rates, thereby allowing two-dimensional NMR experiments to be carried out at very rapid repetition rates (i.e., 5 s^{-1}). (3) The heme proton hyperfine resonance pattern for this paramagnetic form of wild-type monomer hemoglobin component IV provides an analytical reference for the integrity of the heme active site. This is anticipated to facilitate rapid analysis of subsequently produced recombinant derivatives of this protein. (4) The cyanide-ligated protein has a heme pocket structure similar to those of the O_2- and CO-ligated forms of the physiologically important, reduced form of the protein, so that the heme and proximal histidine proton assignments will serve as a basis for further assignments within the heme binding site. Complete assignments, in combination with recombinant derivatives of this monomer hemoglobin, will give further insight into local interactions that influence ligand binding kinetics and heme orientational isomerism.

Glycera dibranchiata contains three major monomer hemoglobins (II, III, and IV) that are a group of myoglobin-like proteins. Interest in this set of proteins stems from limited sequencing and crystallography results, which revealed that at least one of these proteins has the naturally occurring replacement of its "distal" histidine by leucine (Li & Riggs, 1971; Imamura et al., 1972; Padlan & Love, 1974; Simons & Satterlee, 1989, 1991; Arents & Love, 1989, 1991; Alam et al., 1994). These proteins have a global tertiary architecture very similar to that of sperm whale myoglobin (SWMb[1]) (Padlan & Love, 1974; Arents & Love, 1991; Alam et al., 1994), but they exhibit very different kinetic parameters, equilibrium ligand binding properties (Mintorovitch & Satterlee, 1988; Mintorovitch et al., 1989; Parkhurst et al., 1980), and isoelectric focusing behavior (Constantinidis & Satterlee, 1987; Constantinidis et al., 1989) compared to SWMb.

Work in this laboratory is currently directed toward determining the heme pocket structures of each of the three major wild-type monomer hemoglobins, as well as toward expressing, purifying, and characterizing recombinant mutant proteins derived from the monomer component IV hemoglobin (GMH4). NMR spectroscopy is a valuable tool in both of these efforts, and initially, we have chosen to concentrate on the oxidized (i.e., met-), cyanide-ligated form of monomer hemoglobin component IV (metGMH4CN) for several reasons. First, metGMH4CN is paramagnetic by virtue of a single unpaired electron formally associated with the heme iron ion ($S = {}^1/_2$), which causes increased chemical shift dispersion via hyperfine shifts for protons located within the heme active site. This may simplify initial protein characterization compared to the effort required by NMR studies of the diamagnetic forms of GMH4 (Satterlee, 1986; Cooke & Wright, 1985a,b; Cooke et al., 1987). Second, the observed hyperfine shifts in low-spin metGMH4CN contain significant dipolar contributions (La Mar & Walker, 1979; Satterlee, 1986, 1990a,b), so that the hyperfine-shifted proton resonances include those from amino acids within the active site, not just the heme. Differential identification of heme and proximal histidine resonances of the major form of metGMH4CN among the many hyperfine-shifted resonances is the first step in acquiring information on its heme site structure and a prerequisite for making specific assignments of amino acids close to the heme. Third, the observed proton hyperfine shift pattern is very sensitive to heme–protein contacts and heme electronic structure, as well as to more subtle structural parameters, such as conformationally induced changes in the

† This work is supported by the National Science Foundation (DMB9018982). Support for the NMR instrumentation at WSU came from the NIH (RR06312011) and from the Battelle Pacific Northwest Laboratory. We gratefully acknowledge use of the Protein Data Bank at Brookhaven National Laboratory.

* Author to whom correspondence should be addressed. Telephone: (509)335-8620. FAX: (509)335-8867. e-mail: hemeteam@cosy.chem.wsu.edu.

‡ Department of Biochemistry and Biophysics.

§ Department of Chemistry.

® Abstract published in *Advance ACS Abstracts,* March 15, 1994.

[1] Abbreviations: GMG4, *Glycera dibranchiata* monomer component IV globin; GMH4, *Glycera dibranchiata* monomer component IV hemoglobin; metGMH4, oxidized (i.e., ferric) form of GMH4; metGMH4CN, oxidized, cyanide-ligated form of GMH4; Mb, myoglobin; SWMb, sperm whale myoglobin; metSWMbCN, oxidized, cyanide-ligated form of sperm whale Mb; CM, carboxymethyl; COSY, correlated spectroscopy; NOESY, two-dimensional nuclear Overhauser effect spectroscopy; 1D NOE, one-dimensional nuclear Overhauser effect; SUPERWEFT, standard inversion recovery T_1 experiment under fast recycle rates; DSS, 2,2-dimethyl-2-silapentane-5-sulfonate.

0006-2960/94/0433-4008$04.50/0

magnetic axes of the ferric heme and local dynamics (Lecomte & La Mar, 1987; Qin et al., 1992, 1993; Emerson & La Mar, 1990; Rajarathnam et al., 1992; Cutnell et al., 1981; Allocatelli et al., 1993; Yamamoto & Suzuki, 1993). Consequently, even small differences in the heme pocket structure in expressed proteins should be readily detectable in the oxidized, metcyano forms. However, achievement of these results first requires an extensive, reliable set of proton assignments for the heme pocket, including the heme and the proximal histidine.

A potential complicating feature is that the observed shift dispersion for metGMH4CN is significantly less than those for the cyanide-ligated forms of other well-studied myoglobins such as sperm whale (Emerson & La Mar, 1990a,b; Yu et al., 1990), *Aplysia limacina* (Peyton et al., 1989; Qin et al., 1992), *Dolabella auricularia* (Yamamoto & Suzuki, 1993), and shark (Yamamoto et al., 1989, 1991), as well as a majority of other unrelated heme proteins. This smaller observed shift dispersion severely challenges attempts at assigning the heme and proximal histidine protons in metGMH4CN, since essentially the same number of hyperfine-shifted resonances that occur in other low-spin metmyoglobins are crowded into a smaller range. The hyperfine shift pattern is further complicated by the fact that it consists of both major and minor forms of metGMH4CN (vide infra; Constantinidis & Satterlee, 1987; Constantinidis et al., 1988). In this respect, metGMH4CN provides an excellent test of the utility of recent unorthodox implementations (de Ropp et al., 1991a,b) of standard two-dimensional NMR experiments for the purpose of elucidating nuclear connectivities in proton spin systems that contain rapidly relaxing, hyperfine-shifted protons. We illustrate this by identifying a complete, self-consistent set of assignments for all of the metGMH4CN heme and proximal histidine (His90) proton resonances, most of which lie in the very crowded 0–10 ppm spectral region.

One of the goals of our continuing research program is to identify methods that offer the possibility of rapid comparison of critical structural elements in expressed proteins to those of the native proteins. We are now expressing the recombinant wild-type *Glycera dibranchiata* monomer hemoglobin component IV, as well as distal residue mutant proteins. These mutants are being expressed on the premise that the differential ligation properties seen between GMH4 and SWMb, as well as other genetic variants of SWMb, are controlled in large part by the nature of distal amino acids residing on the E-helix (E7, E10, and E11) and the B-helix (B10). Structural data, along with ligand binding kinetic data, of genetically produced variants at these positions in GMH4 may provide additional insight into the structural regulation of ligand binding dynamics in these non-cooperative heme proteins. The assignments for metGMH4CN presented here provide initial reference data for the future characterization of recombinant derivatives.

MATERIALS AND METHODS

Sample Preparation. Native metGMH4 was prepared and purified from *Glycera dibranchiata* as previously described (Kandler et al., 1984; Constatinidis & Satterlee, 1987), with a small change in the final cation-exchange chromatography conditions. After the initial gel filtration step, the monomer fraction was dialyzed in 10 mM potassium phosphate, pH 6.0, and loaded onto a cation-exchange column (CM-Sepharose, Sigma) equilibrated with the same buffer in order to concentrate the protein. The minor monomer components, Ia and Ib, were eluted with a shallow pH gradient up to pH 6.8. This was followed immediately by a linear gradient from 0 to 10 mM KCl (pH 6.8, 10 mM potassium phosphate) for the purpose of eluting monomer components II and III. Monomer hemoglobin component IV was finally removed from the column by applying a shallow gradient extending to 20 mM KCl. Sperm whale myoglobin was purchased from Sigma and used without further purification.

Cyanomethemoglobin and cyanometmyoglobin complexes, metGMH4CN and metSWMbCN, respectively, were prepared by the addition of excess KCN to the individual proteins following oxidation with potassium ferricyanide (Mallinckrodt). This was followed by extensive washing within an Amicon untrafiltration cell using a buffer composed of 100 mM potassium phosphate/100 mM KCl/ 20 mM KCN (pH′ 6.41) in ^2H_2O (Isotec, 99.9%). For the detection of isotope-exchangeable proton resonances, some samples were maintained in this same buffer, but with a solvent composition that was 90% H_2O/10% ^2H_2O (pH′ 6.80). The designation, pH′, refers to pH measurements made in ^2H_2O buffer solutions with no correction for the isotope effect. All NMR samples had final protein concentrations ranging from 3 to 4 mM.

^1H NMR Experiments. All ^1H NMR spectra were collected on a Varian VXR-500S NMR spectrometer operating in the quadrature detection mode at a nominal proton frequency of 500 MHz. In all 1D and 2D, experiments the water resonance was selectively saturated, as necessary, using the decoupler channel during the relaxation delay period or during both the relaxation delay and evolution periods.

Steady-state 1D NOE difference experiments (Satterlee et al., 1987) were obtained by irradiating the desired resonance for 100–200 ms using the transmitter channel and subtracting this spectrum from an identically obtained spectrum with the transmitter placed off-resonance. From 4000 to 10 000 transients were collected for each set of spectra using a 1-s recycle delay time. Ninety-degree pulse widths typically ranged from 6 to 8 ms. Pre-steady-state one-dimensional NOE difference experiments (Keller & Wuthrich, 1981) were performed in a manner identical to that of the steady-state experiments, with irradiation times ranging from 10 to 100 ms.

Nonselective apparent spin–lattice relaxation times (T_1^{app}) were obtained using a standard inversion recovery sequence (180°–τ–90°–acquire) and were determined from the initial slope of the semilogrithmic plots of the fractional deviation of the z-magnetization from equilibrium versus the relaxation delay time (τ). This type of display more readily depicts multiple-exponential relaxation as deviations from the expected linearity of these plots (Granot, 1982; Satterlee, 1986; La Mar & de Ropp, 1993). In all cases, plots of these data were linear in their initial phases at short delay times (less than 100 ms). Estimates of the spin–spin proton relaxation times (T_2) were obtained from measurements of the unapodized resonance line widths at half height.

A SUPERWEFT (Inubushi & Becker, 1983) pulse sequence was used to suppress the slowly relaxing diamagnetic proton envelope, while allowing preferential observation of the broad, rapidly relaxing protons. This experiment is identical to the inversion recovery experiment used for measuring T_1's, but the interpulse delay (80 ms) was set manually to null the intensity in the diamagnetic region, while a short acquisition time (13–26 ms) and relaxation delay (1–10 ms) allowed effective relaxation of only the quickly relaxing protons near the heme iron.

Table 1: ^1H NMR Parameters for the Assigned Heme Resonances in *Glycera dibranchiata* Monomer IV Metcyanohemoglobin (GMH4CN) in ^2H_2O

resonance	chemical shift[a]	T_1^{app} [b]	T_2[c]	Curie intercepts[d]	slope[e]
1-CH_3	0.64			(15.95)	−4.336
3-CH_3	18.75	190	2.74	3.46	4.507
5-CH_3	6.46			(13.77)	−2.049
8-CH_3	19.88	126	5.40	−3.76	6.796
2α	7.38			(23.55)	−4.556
2βc	−3.79	438	3.03	12.04	−3.095
2βt	−2.37	320	4.94	7.22	−0.852
4α	11.19	422	6.24	11.02	−0.293
4βt	−3.27		8.60	13.27	−2.232
4βc	−4.06	182	5.64	10.01	−7.656
6α1	7.66			(18.06)	−2.950
6α2	−4.38	352	5.39	(12.87)	−4.884
6β1	−2.35		6.63	5.78	−2.306
6β2	0.99			(6.55)	−1.590
7α1	11.13	249	4.61	3.75	2.869
7α2	5.38			(12.37)	−1.995
7β1	−2.67		6.01	7.89	−2.365
7β2	−3.21	278	5.64	10.01	−2.966
His90β1	11.67	150	6.77	(3.17)	−2.395
His90β2	7.14			(4.13)	−.039
His90Cα	8.59			(3.47)	1.444
His90NpH	12.64[f]	149[g]	10.6	(6.72)	1.711
His90NπH	23.66[f]	31[g]	3.9	2.55	6.085
His90C5H	24.7[h]	4.3	0.3	−31.3	16.103
α-meso	−0.17			(8.23)	−2.402
β-meso	−0.78			(7.12)	−1.721
γ-meso	−0.47			(15.19)	−4.432
δ-meso	3.07			(7.80)	−1.554

[a] Chemical shifts are reported at 15 °C pH′ 6.43, in 0.1 M KCl, 0.1 M potassium phosphate, and 20 mM KCN referenced to DSS through residual HDO assigned to 4.67 ppm. [b] T_1^{app} is the apparent spin–lattice relaxation time in milliseconds obtained from the initial slopes of the semilog$_e$ T_1 plots at 35 °C. [c] Estimates of spin–spin relaxation times (T_2) in milliseconds were obtained from line widths at half height at 35 °C ($T_2 \approx 1/\pi\nu_{1/2}$). Peak deconvolution analysis was used in areas of peak overlap. [d] Curie intercepts are the predicted chemical shifts at infinite temperature and are estimated by extrapolating the linear least-squares fit Curie lines to $1/T$ (K) = 0. This is an estimate of the chemical shift with no paramagnetic contribution. Numbers in parentheses denote data obtained using NOESY spectra at several temperatures. [e] Slopes (ppm·K) × 10^3 from plots of observed shift versus reciprocal absolute temperature (K). [f] Chemical shift recorded in 90% H_2O buffer (pH 6.81). [g] T_1^{app} data recorded at 35 °C in 90% H_2O/10% D_2O buffer at pH′ 6.81. [h] Chemical shift recorded at 20 °C due to overlap at 15 °C.

A pulse sequence that included a binomial read pulse (Hore, 1983) was used to record 1D ^1H spectra of all protein samples in 90% H_2O/10% D_2O.

Several adaptations were made within standard 2D NMR methods to accommodate the paramagnetic nature of metGMH4CN. Due to the short T_1's and shorter T_2's seen in metGMH4CN (Table 1), transverse magnetization is quickly lost during mixing and acquisition times. This is a result of the paramagnetic contribution to the proton nuclear relaxation (Swift, 1973; La Mar & Walker, 1979; Satterlee, 1986, 1990a,b; La Mar & de Ropp, 1993). To minimize these limitations, NOESY experiments were performed with short mixing times and short acquisition times. Shorter acquisition times (20–40 ms) were introduced by using a smaller number of points (1024) over the spectral width of interest (20 000 Hz). Whereas this lowers the digital resolution, the larger spectral dispersion and larger hyperfine resonance line widths of metGMH4CN compared to diamagnetic proteins make this less critical for successful hyperfine resonance assignments. In addition, very rapid recycle rates (see below) allowed the effective relaxation of only protons with shorter T_1's and facilitated the rapid accumulation of spectra with sufficient signal/noise levels. Data were processed with window functions that enhanced the portions of the free induction decay associated with the rapidly relaxing protons (details will be discussed later).

Proton homonuclear magnitude COSY (MCOSY) and phase-sensitive COSY spectra (Aue et al., 1976; Wuthrich, 1986) were collected over a range of temperatures (5–35 °C) using spectral widths of both 20 000 and 14 000 Hz. In the process, 1024 complex t_2 points were collected for each of 512 t_1 blocks using 256 transients in each block. Residual water was saturated with the decoupler during the relaxation delay period. Repetition rates of 5, 10, and 15 s^{-1} were used to preferentially suppress the more slowly relaxing diamagnetic resonances.

Proton homonuclear phase-sensitive 2D NOE (NOESY; Kumar et al., 1981) spectra were collected over spectral widths of 20 000 and 14 000 Hz, also using 1024 complex t_2 points in 256 t_1 blocks. In each block, 256 transients were sum-averaged, and quadrature detection along t_1 was achieved using the States–Haberkorn–Reuben method (States et al., 1982). Mixing times were varied in a series of separate experiments from 2 to 100 ms for documenting NOE buildups. NOESY experiments were collected at several temperatures between 5 and 35 °C for unambiguous identification of hyperfine-shifted resonances and for obtaining Curie data. Each of the variable-temperature NOESY experiments had a mixing time of 40 ms. A recycle rate of 5 s^{-1} was employed in these cases.

All 1D and 2D data were processed on either a Sun Microsystems Sparcstation using the Varian VNMR software (Palo Alto, CA) or a Personal Iris (SGI) using the program Felix (Hare Research, V2.1). MCOSY data were processed using an unshifted sine-bell-squared function in both the t_1 and t_2 domains. These data were processed over either 256, 512, or 1024 points in the t_2 domain and over 256 or all points in the t_1 domain. In all cases, the data sets were zero-filled to 2048 × 2048 points before Fourier transformation.

NOESY spectra were processed using a 30-deg-shifted, sine-bell-squared window function in both dimensions. The apodization functions were applied over 256 or 512 points in the t_2 dimension and over 256 or 512 points in t_1. Again, all data sets were zero-filled to 2048 × 2048 points before transformation. All chemical shifts were referenced to DSS through the residual water signal, which was assigned the chemical shift of 4.67 ppm.

Crystal Structure. Fe^{2+}–proton distances were measured within the CO form of the monomer hemoglobin (Arents & Love, 1989, 1991; Berenstein et al., 1977) using the software package INSIGHTII (version 2.1, BIOSYM). Hydrogens were added to the crystal structure using the same software. The monomer hemoglobin crystal structure does not correspond to the primary sequence for GMH4, and as a result, the three-dimensional model structure of GMH4 was also used in making pertinent structural correlations (Alam et al., 1994).

RESULTS AND DISCUSSION

General Spectral Features. Figure 1 shows the modified Fischer heme labeling scheme (Moss, 1988) that is used to describe heme and proximal histidine labeling in this work. This figure is presented not only as a reference for discussion of the results presented here but also to illustrate the two different heme rotational isomers present in SWMb and GMH4. X-ray crystal structures of a *Glycera dibranchiata* monomer hemoglobin (Arents & Love, 1989) and SWMb (Kuriyan et al., 1986) revealed that the heme orientation in

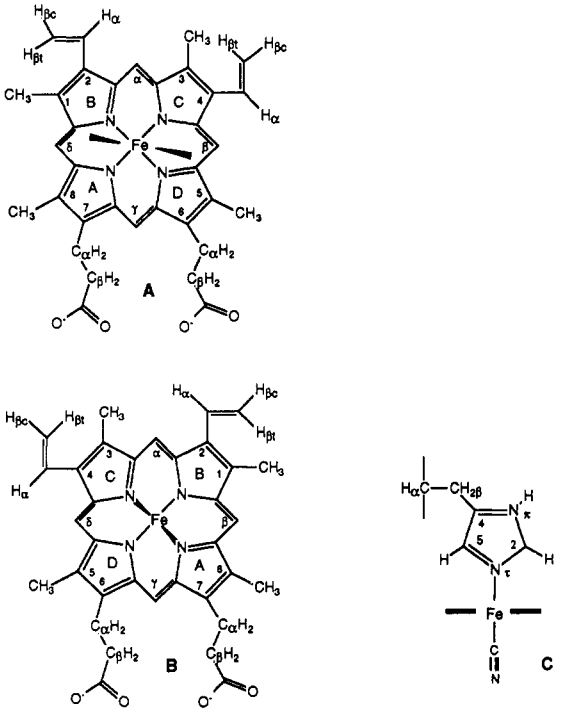

FIGURE 1: Heme b viewed from the proximal side (A and B) and the coordinated proximal histidine (C), showing the conventional labeling system. The dark wedges show the projection of the proximal histidine onto the heme plane for GMH4 (A) and SWMb (B). Notice that heme rotational disorder arises from a rotation about the α–γ meso axis.

GMH4 is rotated 180° about the α–γ meso axis compared to SWMb (Arents & Love, 1989; Kuriyan et al., 1986; Cooke & Wright, 1985a,b; Mintorovitch et al., 1990). These structures are shown in Figure 1. In addition, both myoglobin and the monomer hemoglobin have been found to possess minor forms in solution due to this heme rotational isomerism (Jue et al., 1983; La Mar et al., 1984; Lecomte et al., 1985; Constantinidis et al., 1988). In GMH4, the major protein form is present to the extent of 85–90% in solutions used for NMR studies (Mintorovitch et al., 1990; Constantinidis et al., 1988).

The proton 1D NMR spectrum of native metGMH4CN is generally similar to that of metSWMbCN, but critical inspection reveals many specific differences. To illustrate this, the resolved proton hyperfine-shifted regions are shown for both metSWMbCN (Figure 2A) and metGMH4CN (Figure 2B–D). Previous proton assignments for metSWMbCN are indicated in Figure 2A (Emerson & La Mar, 1990a,b; Yu et al., 1990). Figure 2B presents the spectrum of metGMH4CN at the same temperature as in Figure 2A. Figure 2C is the metGMH4CN spectrum at 35 °C, with some of the proton assignments for metGMH4CN shown. Figure 2B,C is presented to illustrate the significant temperature-dependent shifts and resonance line-width narrowing. The specific cause of this temperature-dependent narrowing is now under investigation, with preliminary evidence pointing to reorientation of at least two different amino acid side chains in the heme pocket. Figure 2D shows a portion of the SUPERWEFT spectrum for metGMH4CN at 35 °C, in which two very broad, extremely fast relaxing, high-frequency resonances are emphasized. It should be noted that the shift values reported in Tables 1 and 2 are those at 15 °C.

Figure 2A,B shows the substantially smaller proton hyperfine chemical shift dispersion present in metGMH4CN

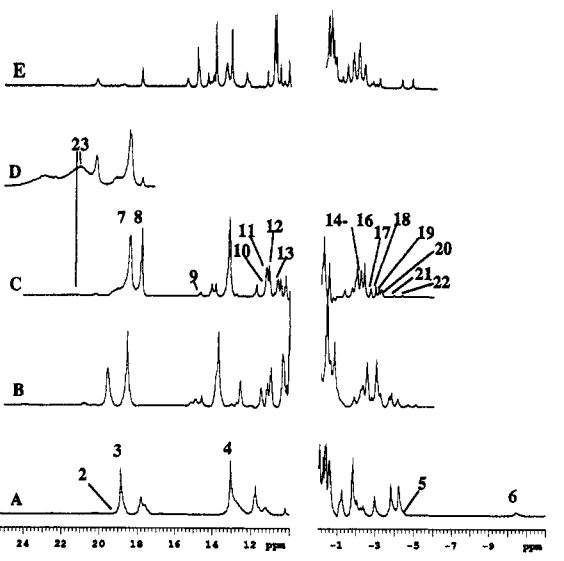

FIGURE 2: 500-MHz 1D ^{1}H NMR spectra of GMH4CN and SWMbCN in ^2H_2O (pH′ 6.42). (A) SWMbCN recorded at 20 °C with some of the previously assigned resonances included above the spectra: (1) 5-CH_3; (2) H93C5H; (3) 1-CH_3; (4) 8-CH_3; (5) H93C2H; (6) I99CδH. (B) GMH4CN recorded at 20 °C. (C) GMH4CN at 35 °C with assignments of the resolvable heme resonances arising from this work labeled above the spectra: (7) 8-CH_3; (8) 3-CH_3; (9) 2α'; (10) 1-CH_3'; (11) 4α; (12) H90β_1H; (13) 7α1; (14) 2βt and 6β1; (15) 7β1; (16) 4β_t; (17) 7β2; (18) 4β_c; (19) 2β_c; (20) 6α2; (21) 2β_c'; (22) 2β_t'; (23) H90C5H. (D) The trace for GMH4CN collected using the SUPERWEFT experiment at 35 °C, emphasizing the fast relaxing proximal His90C5H. (E) A recombinant mutant form (rec-gmg) of GMH4 exhibiting increased amounts of rotational disorder (35 °C).

Table 2: ^{1}H NMR Parameters for the Assigned Minor Form Resonances in *Glycera dibranchiata* Monomer IV Metcyanohemoglobin (GMH4CN) in ^2H_2O

resonance	chemical shift[a]	T_1^{app} [b]	T_2[c]	Curie intercepts[d]	slope[e]
1-CH_3'	11.72		4.3	1.92	2.769
2α'	15.31	166	7.7	5.69	2.727
2βt′	−4.88	277	7.9	10.29	−4.424
2βc′	−5.31	260		9.82	−4.158
His90β1′	11.90			3.01	2.551
His90β2′	7.38			(4.86)	0.731
His90NπH′	23.99	29	3.6	0.83	6.789
His90C5H′	25.9				
His90Cα'	8.93			(3.83)	1.446

[a] Chemical shifts are reported at 15 °C, pH′ 6.43, in 0.1 M KCl, 0.1 M potassium phosphate, and 20 mM KCN referenced to DSS through residual HDO assigned to 4.67 ppm. [b] T_1^{app} is the apparent spin–lattice relaxation time in milliseconds obtained from the initial slopes of the semilog$_e$ T_1 plots at 35 °C. [c] Estimates of spin–spin relaxation times (T_2) in milliseconds were obtained from line widths at half height at 35 °C ($T_2 \approx 1/\pi\nu_{1/2}$). Peak deconvolution analysis was used in areas of peak overlap. [d] Curie intercepts are the predicted chemical shifts at infinite temperature and are estimated by extrapolating the linear least-squares fit of Curie lines to $1/T$ (K) = 0. This is an estimate of the chemical shift with no paramagnetic contribution. Numbers in parentheses denote data obtained using NOESY spectra at several temperatures. [e] Slopes (ppm·K) × 10^3 from plots of observed shift versus reciprocal absolute temperature (K).

(Figure 2B), which for the major resonances amounts to only 26 ppm (−5 to ~21 ppm in D_2O) at 20 °C. For metSWMbCN at the same temperature the dispersion is 39 ppm (−10.5 to 28 ppm) (Figure 2A). In addition, metGMH4CN has only two well-resolved heme methyl resonances that lie outside the crowded 0–10 ppm region (8-CH_3 and 3-CH_3), and their near overlap indicates that both are in nearly identical magnetic environments (Figure 2C). This situation significantly differs from the observation of three well-resolved heme methyl

resonances (the 5-, 1-, and 8-methyls, Figure 2A) observed for metSWMbCN (Emerson & La Mar, 1990a,b; Yu et al., 1990) and the myoglobins from *Aplysia limacina* (Peyton et al., 1989; Qin et al., 1992), *Dolabella auricularia* (Yamamoto & Suzuki, 1993), and *Galeorhinus japonicus* (Yamamoto et al., 1989, 1991).

Apart from the hyperfine proton resonances associated with the major metGMH4CN form shown in Figure 2, one can also detect several of the metGMH4CN minor form resonances (peaks 1-CH_3', 2-Hα', 2-H$\beta c'$ and 2-H$\beta t'$). Evidence of the heme orientation difference between metGMH4CN and metSWMbCN is given by the pattern of heme methyl resonances. For metGMH4CN, the heme 8-CH_3 and 3-CH_3 resonances occur at the highest frequencies, whereas in metSWMbCN it is the 5-CH_3 and 1-CH_3 resonances. An important result from this work is that a minor form existing simultaneously in solution with the major form does not compromise our ability to make assignments for the major form. Several minor form assignments are also presented to indicate that we can clearly differentiate the two sets of resonances.

Comparison of the proton 1D NMR spectra in Figure 2 also shows that metGMH4CN lacks the extreme low-frequency resonance attributed to the Cγ-H of the highly conserved Ile99 in metSWMbCN (FG5). The crystal structure of a *Glycera dibranchiata* monomer hemoglobin CO (Padlan & Love, 1974; Arents & Love, 1989), earlier protein sequencing of the monomer fraction (Imamura et al., 1972), recently completed protein sequencing of this component IV globin (GMG4), and a model structure of GMH4 (Alam et al., 1994) all suggest that a corresponding Ile is present on the proximal side of the heme in GMH4 (Ile98). The absence of this peak in the proton NMR spectrum of metGMH4CN indicates that it experiences a different magnetic environment in metGMH4CN, due either to a decrease in rhombic magnetic anisotropy or to different physical positioning. In this respect, metGMH4CN resembles the CN-ligated shark metmyoglobin (*Galeorhinus japonicus*; Yamamoto et al., 1991).

Hyperfine Resonance Assignments: General Approach. A complete set of heme proton resonance assignments was made using a logical suite of 1D and 2D proton NMR experiments that take advantage of special properties of hyperfine-shifted proton resonances: short relaxation times (i.e., rapid relaxation rates) and large temperature dependencies. These included T_1 determinations for non-overlapping resonances, 1D NOE difference spectroscopy, SUPERWEFT, NOESY, and MCOSY. Many of these experiments were performed at several temperatures covering a 35-deg temperature range. This was done in order to take advantage of the significant temperature dependencies of hyperfine-shifted resonances, to resolve peak overlaps in crowded spectral regions, and to make unambiguous identifications of true hyperfine-shifted resonances. Many of the metGMH4CN heme hyperfine-shifted resonances occur within the crowded 0–10 ppm range, but we found it possible to differentially enhance the cross-peak intensities of the rapidly relaxing hyperfine-shifted protons within this "diamagnetic" region by using very short recycle times (i.e., rapid repetition rates). This preferentially suppressed the intensities of the slowly relaxing diamagnetic proton resonances to a significant extent and is essentially a "partial differential relaxation" filter (de Ropp et al., 1991a,b).

The starting points for these assignments were the previously assigned (major form) heme 3-CH_3, 8-CH_3, and 4-vinyl Hα resonances (Mintorovitch et al., 1990). As with diamagnetic molecules, we first identified and classified spin systems of

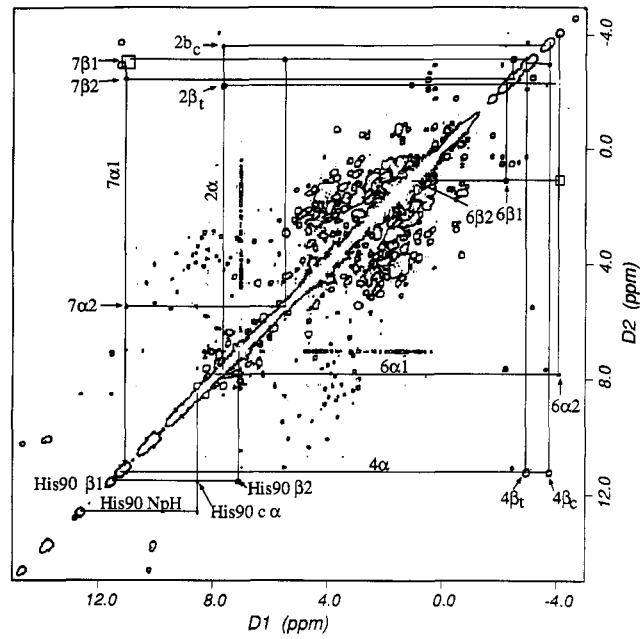

FIGURE 3: ^1H–^1H magnitude COSY (MCOSY) spectra of GMH4CN collected at 20 °C in ^2H_2O (pH′ 6.42). The expanded region (16 to −6 ppm) outlines the 2-vinyl, 4-vinyl, 6-propionate, 7-propionate, and proximal His90 (CαH, CβH, and NpH) groups. Standard heme labels are used as illustrated in Figure 1. Boxes indicate correlations observed at lower contour levels.

the heme vinyl and propionate substituents using COSY and NOESY experiments (de Ropp et al., 1991a,b; Satterlee & Erman, 1991; Yamamoto et al., 1989, 1991). Then, additional NOE connectivities to neighboring protons were used to assign substituents to a given heme pyrrole. Next, NOE connectivities between substituents on adjacent pyrroles and NOE connectivities from pyrrole substituents to meso protons (Figure 1) were used to confirm the specific pyrrole substituent group positions and to assign the meso proton resonances. Finally, the combination of spin–lattice relaxation time (T_1^{app}) measurements, Curie plots of variable-temperature shift data, and 2D NOE buildup curves was used to confirm assignments.

As will be described later, the combination of NOESY and COSY experiments also aided in assigning the stereochemistry of the two heme vinyl groups and the propionic acid side chains relative to neighboring heme methyls. In the discussion that follows, the numerical values for the observed shifts described in the text are the values at 15 °C, as reported in Tables 1 and 2. All spectra are presented at temperatures that reduce the overlap of resonances of interest and are noted in the figure legends.

Heme Assignments. (a) Vinyl Groups. Experience with other paramagnetic heme proteins has shown that heme vinyl groups demonstrate characteristic, three-resonance hyperfine shift patterns (Yamamoto et al., 1989; Emerson & La Mar, 1990a,b; Yu et al., 1991; Satterlee & Erman, 1991; Satterlee et al., 1991; de Ropp et al., 1991a). We describe in detail the heme 4-vinyl assignments for the major form of metGMH4CN. This procedure begins with the assigned 4α-proton (11.19 ppm), which can be used as a starting point to assign the two 4β-protons. In the MCOSY (Figure 3), phase-sensitive COSY (not shown), and NOESY (Figure 4) contour plots, the 4Hα resonance displays two cross peaks that are significantly shifted to lower frequency (−3.27 and −4.06 ppm), which is typical for β-vinyl protons in low-spin ferriheme proteins (Yamamoto et al., 1989; Emerson & La Mar, 1990a,b; Yu et al., 1991; Satterlee et al, 1991; de Ropp et al., 1991a; Satterlee & Erman, 1991). These have been assigned as the

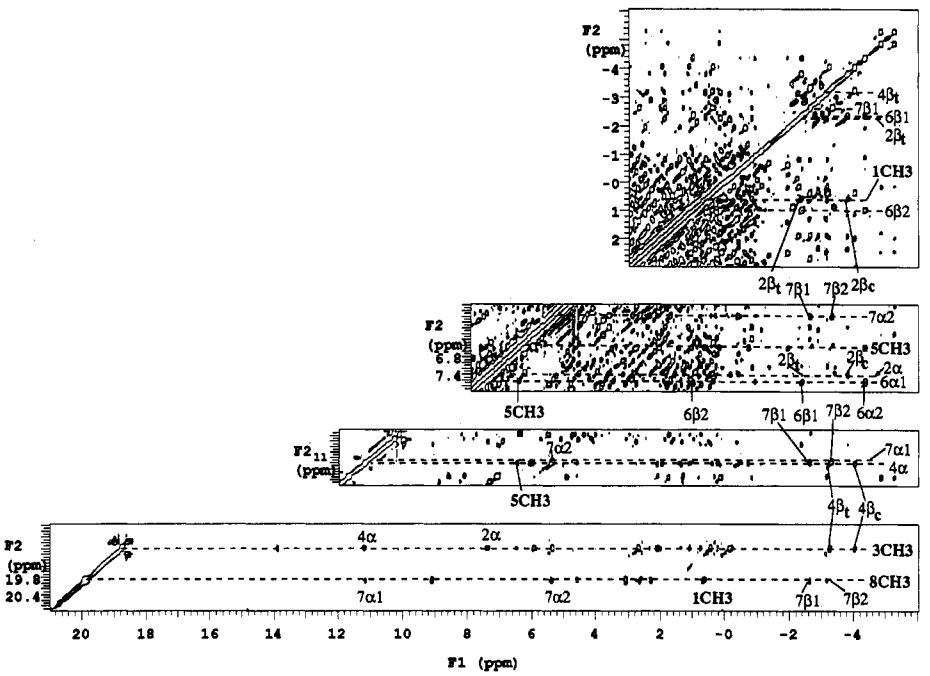

FIGURE 4: Composite NOESY map collected at 40-ms mixing time for GMH4CN in ^2H_2O (pH' 6.42) at 15 °C. All intra-pyrrole NOEs used for heme substituent assignments are included. For the resolved 8-CH_3, 3-CH_3, 4α, 7α1, 2α, 6α1, 5CH_3, 7α2, 6β2, 1CH_3, 2β_t, 6β1, and 4β_t (shown by horizontally dashed lines), the f_2 resonance assignments are labeled at the end of the dashed lines. Cross peaks are labeled above or below the dashed lines as needed.

4β_{trans} (4βt) and the 4β_{cis} (4βc) protons, respectively, on the basis of their relative cross-peak intensities (Figures 3 and 4) and the expected coupling constants to 4Hα (19 and 11 Hz, respectively; Harris, 1983; La Mar & de Ropp, 1993). A second three-resonance spin system of the major protein form has been assigned as the 2-vinyl group [2α (7.38 ppm), 2βc (−3.79 ppm), and 2βt (−2.37 ppm)] in a similar manner (Figures 3 and 4, Table 1).

When COSY experiments were carried out under extremely fast recycling conditions (i.e., 10 −15 s^{-1}), an additional vinyl pattern occurred along a slice at 15.31 ppm (vinyl Hα), exhibiting vicinal couplings to the Hβt (−4.88 ppm) and Hβc (−5.31 ppm) with the expected Hβt/Hβc connectivity found in the low-frequency region. The relative intensity of this set of resonances in the 1D spectra suggests that this spin system is the minor form of metGMH4CN. Considering the heme orientation of this minor form, it is assigned as the 2′-vinyl spin system (Table 2).

(b) Propionic Acid Groups. In addition to the obvious three-proton spin systems described above, there were also two four-proton spin systems evident within the MCOSY spectra that met all of the other criteria for hyperfine-shifted resonances (Table 1). These arise from the 6- and 7-propionic acid side chains, since these are the only remaining heme substituents that can form scalar-coupled networks (Figure 1). The highest frequency resonance of the eight (11.13 ppm) was initially assigned to a 7α-proton (7-Hα1) on the basis of the observation that its neighboring substituent on heme pyrrole D, the 8-CH_3 (Figure 1), displayed the highest frequency heme methyl resonance shift (19.88 ppm; Figure 2B,C). The resonance at 11.13 ppm shows scalar coupling to three other resonances (Figure 3). The most intense cross peak arises from its geminal partner (7-Hα2) at 5.38 ppm. Smaller scalar couplings arise from the 7β-protons at −2.67 (7-Hβ1) and −3.21 ppm (7-Hβ2). Additionally, a strong 7β1–7β2 cross peak is observed.

Another four-proton spin system can be easily identified in these spectra and was initially assigned to the 6-propionic acid side chain by elimination. The highest frequency resonance of this spin system (6-Hα1, 7.66 ppm) exhibits an MCOSY cross peak to one other resonance. This intense cross peak is presumably its geminal partner, 6-Hα2, at −4.38 ppm. The latter couples strongly to a resonance at 0.99 ppm which corresponds to the 6-Hβ2, which was coupled strongly to 6β1 at −2.35 ppm.

Intra-pyrrole NOE Connectivities. Using the previous heme 8-methyl and 3-methyl assignments for metGMH4CN (Mintorovitch et al., 1990) and the classification of spin systems described above, a self-consistent pattern of NOE connectivities within substituent groups and between different substituent groups on the four heme pyrroles could be traced for the major metGMH4CN form. Some of these are shown in Figure 4. For example, the 8-CH_3 resonance showed NOE connectivities to the previously identified 7α1-, 7α2-, 7β1-, and 7β2-protons (Figure 4), thereby reinforcing their first-stage assignments. The NOE cross peak to the 7-Hα2 is of much greater intensity than is the cross peak to the 7-Hα1, and this indicates that the 7-Hα2 proton is oriented more toward the 8-CH_3 than is the 7-Hα1. Using the same reasoning, the 7-Hβ1 proton is oriented more toward the 8-CH_3 than is the 7-Hβ2.

Other intra-pyrrole dipolar interactions included those between the 3-CH_3 and the 4-vinyl and NOEs within the spin system of the 6-propionate (6α1–6α2, 6α1–6β1, 6β1–6β2, and 6α2–6β1) and within the 2-vinyl group (2α–2βc and 2α–2βt), all of which support their assignments based on COSY data. Within the vinyl groups the individual assignments of Hβc and Hβt relied upon the relative cross-peak intensities in COSY and NOESY experiments, which revealed a 4-vinyl orientation in which the 4-Hα is directed away from the 3-CH_3 and preferably points toward the β-meso proton, as shown in Figure 1.

In addition, a strong NOE was observed from the 6α2 that was proposed to arise from the 5-CH_3 (6.46 ppm). A strong NOE was observed from the 2βt to a resonance proposed to arise from the 1-CH_3 (0.64 ppm), with a weaker NOE from the 2α to the same resonance (Figures 4 and 5). Additional

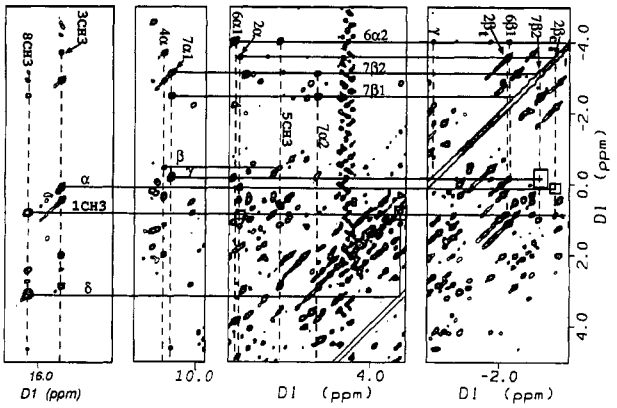

FIGURE 5: Resolved low-field region of the NOESY spectrum (20-ms mixing time) of GMH4CN in ^2H_2O (pH′ 6.42) at 15 °C, illustrating all meso-to-heme periphery dipolar connectivities. The data were processed by applying a 30-deg-shifted sine-bell-squared window function over 256 t_2 × 512 t_1 points prior to zero-filling to 2048 × 2048 points and Fourier transformation. Boxes around the α-meso to $2\beta_c$, γ-meso to $7\beta_2$, and 1-CH_3 to 2α cross peaks highlight correlations seen at lower contours, while the box around the δ-meso to 1-CH_3 correlation emphasizes the crowded region of the expected cross peak. All meso protons are labeled with the single letters, α, β, γ, and δ, respectively.

substantiation of these assignments results from inter-pyrrole NOEs.

NOE Connectivities between Pyrrole Substituents. The 6-propionate assignments gain support from the observation of a common NOE partner for the 6α1-, 6α2-, 7α1-, and 7α2-protons which, to anticipate further results, is assigned to the γ-meso proton (–0.47 ppm). The α- and β-meso proton assignments readily emerged from the variable-temperature NOESY data, which produced spectra like that shown for one of the temperatures (15 °C) in Figure 5. More complete data supporting all meso proton assignments are derived from Curie data and NOE buildup experiments, which will be discussed later.

The 5-methyl assignment proposed above is supported by the following connectivities, which were found in contour plots shown in Figure 4. Both the 6-Hα1 resonance and the proposed 6-Hβ2 resonance show substantial NOEs to the proposed 5-CH_3 (6.46 ppm) which, in turn, shows a weak NOE cross peak to the 4-Hα resonance. These results are consistent with the heme 4-vinyl orientation determined above (Figure 1). Additional support for this 5-CH_3 resonance assignment comes from its NOE connectivity to the proposed β-meso resonance (0.78 ppm), which also experiences an NOE to the 4α-proton (Figures 4 and 5).

At this point in the analysis, only the heme 1-CH_3, on heme pyrrole B, remained unidentified. The other pyrrole B substituent, the 2-vinyl group, was tentatively assigned by COSY experiments, and the assignment was further supported by NOESY spectra. Regardless of the specific heme 2-vinyl orientation, some of the 2-vinyl protons would be expected to display NOE connectivities to the heme 3-methyl resonance and the α-meso proton (Figure 1). The proposed 2-Hα resonance assignment is consistent with this expectation; it displayed a weak cross peak to the 3-CH_3 resonance and a strong cross peak to the proposed α-meso at –0.17 ppm (Figures 4 and 5). No similar connectivity pattern for the 3-methyl could be discerned for the 2β-protons which, combined with the weak 2-Hα/3-CH_3 cross peak, provides evidence for the 2-vinyl orientation shown in Figure 1.

The heme 1-CH_3 resonance, which is buried within the diamagnetic envelope, was the most difficult assignment. On the basis of its position on the heme (Figure 1), it would be expected to display primary NOE connectivities at least to the δ-meso (strong), the 8-CH_3 (weak), and the 2-Hβt (intermediate–strong). We have identified a resonance that fulfills all of these requirements (0.64 ppm), which shows a very weak NOE cross peak to the 8-CH_3 resonance and stronger NOEs to both of the 2-Hβ resonances (–3.79 and –2.37 ppm). In addition, the 1-methyl resonance displays a very weak NOE to the 2α. The 1-CH_3/δ-meso cross peak lies within a very crowded region of the spectrum, so that we cannot be certain that this is a unique set of connectivities, and this assignment remains tentative. However, if this is the heme 1-CH_3 resonance, then the observed pattern of NOE cross-peak intensities indicates that the 2-vinyl may adopt an orientation that is not as strictly parallel to the heme plane as the connectivities discussed in the preceding paragraph might imply.

Assignment of the 6-propionate spin system is not wholly satisfying in that each of the protons in the spin system does not exhibit mutual scalar coupling connectivity to the others, as is the case for the 7-propionate spin system. Also, the observed shift difference for the two 6-Hα resonances is larger than expected. However, observation of common NOE cross peaks among these proton resonances (Figures 4 and 5), their temperature dependence, and their T_2's (Table 1) support the spin system assignment. These NMR differences between the propionic acid side chains parallel structural differences. In both the crystal structure of the *Glycera dibranchiata* monomer CO–hemoglobin (Arents & Love, 1989) and the model structure of GMH4 (Alam et al., 1994), the 6-propionate and 7-propionate adopt quite different conformations. The 6-propionate is highly bent in order to form a hydrogen bond, whereas the 7-propionate does not internally hydrogen bond but adopts an extended conformation and may be quite mobile. The bent nature of the 6-propionate side chain may cause the large chemical shift difference for the 6-Hα-protons and the lack of scalar coupling between the 6α1- and β-protons.

Meso Proton Assignments. Likely candidates for three of the four meso proton resonance assignments were made using NOE connectivities to other heme peripheral substituents (Figure 5). Only the δ-meso assignment remained ambiguous, in part due to ambiguity in the heme 1-CH_3 resonance assignment described above and to the crowded spectral region in which both the δ-meso and 1-CH_3 reside (3.07 and 0.64 ppm). An effort to solidly identify all heme meso proton candidates utilized variable-temperature NOESY experiments in combination with NOESY buildup experiments. The goal was to identify primary NOEs between the meso protons and their nearest neighbors. For diamagnetic molecules, analyses of NOE rise-curve initial slopes are the only quantitative means of determining the pairwise internuclear cross-relaxation rate (σ_{ij}). These types of experiments are the key to quantitating relative internuclear distances (Macura et al., 1981; Ernst et al., 1986; Neuhaus & Williamson, 1989; Yip, 1990; La Mar & de Ropp, 1993). The concept is a simple one—nearest neighbors display larger NOEs at shorter mixing times. However, for paramagnetic proteins such as metGMH4CN, these measurements are complicated by the following factors: very short nuclear T_1's and substantial spin diffusion (La Mar & de Ropp, 1993). In metGMH4CN, identification of primary NOEs cannot be made using steady-state NOE experiments due to the presence of spin diffusion. Furthermore, since T_1 relaxation competes with the NOE buildup (de Ropp et al., 1991a; La Mar & de Ropp, 1993), the maximum magnitude of an observed NOE is reached on the

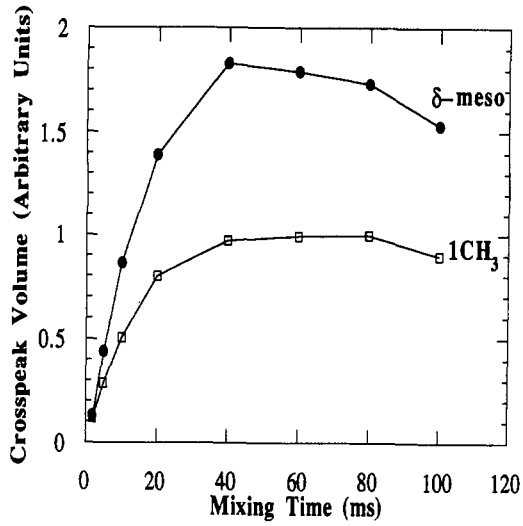

FIGURE 6: NOE buildup curves (cross-peak intensity (height, arbitrary units) versus mixing time (ms)) for 1-CH_3. The best candidate for the δ-meso is also labeled. NOE buildup data for all NOEs observed for the 8-CH_3 are included in the supplementary material. These include meso candidates a, b, and c from the Curie plots (Figure 7).

order of 100 ms or less for the hyperfine-shifted resonances of metGMH4CN. For this reason, NOE rise curves from NOESY spectra were obtained with short mixing times (<40 ms). The initial slopes of NOE rise curves for many of the unambiguous assignments gave good qualitative indications of the relative distances and were used within this work as indicators of nearest neighbors to heme substituents and to identify meso proton candidates.

For example, we used NOE buildup data, such as that shown in Figure 6, to identify the most likely heme δ-meso resonance. On the basis of the heme structure (Figure 1), the δ-meso should display primary NOEs to the 8-methyl (2.17 Å away) and the 1-methyl (2.25 Å away). Furthermore, the GMH4 model structure (Alam et al., 1994) predicts that the CαH of Phe45 could be equally close to the 8-methyl and show a primary NOE to it. We were able to identify three temperature-dependent primary NOE partners (a, b, and c in the supplementary material) to the 8-methyl (in addition to the tentatively assigned 1-methyl resonance). The resonance assigned to the δ-meso was selected on the basis of its NOEs to both the 8-CH_3 and 1-CH_3 and the fact that it displayed no scalar connectivity (as peak c does). The resonance labeled c in the supplementary material (and Curie data; Figure 7) is tentatively assigned to Phe45 on the basis of its NOE to the 8-methyl, but not the 1-methyl, and the fact that it exhibits scalar connectivity (to 13.7 ppm). Figure 6 is also illustrative of the relatively short time period over which nuclear Overhauser enhancements persist for the heme hyperfine-shifted resonances in this protein.

Next, temperature dependence was considered. Meso proton resonances should exhibit significant temperature dependencies, with extrapolated intercepts at $(1/T) = 0$ (the Curie intercept, Table 1) at about 8–10 ppm. These data are presented in the form of a Curie graph (graph of observed shifts versus inverse temperature), as shown in Figure 7. Extrapolated Curie intercepts estimated from these data are shown in Table 1. Four candidates for assignment as the δ-meso proton emerged from the Curie data shown in Figure 7, but only the peak labeled δ-meso (3.07 ppm) showed both a steep NOE rise curve and a Curie intercept consistent with assignment as a meso proton. This same procedure was followed for the α-, β-, and γ-meso protons.

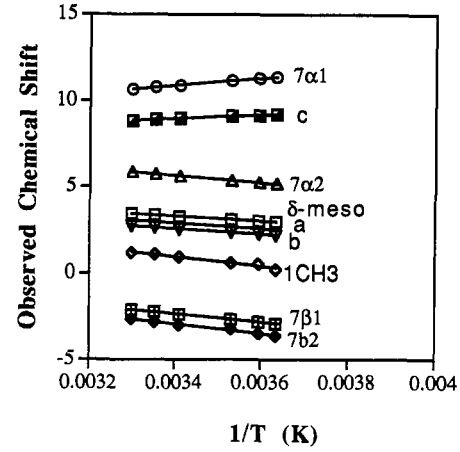

FIGURE 7: Curie plots of all resonances that experience NOEs to the 8-CH_3. Plots of observed chemical shift versus $1/T$ (K) are given as derived from NOESY spectra and 1D spectra recorded at several temperatures ranging from 7 to 35 °C. The assigned resonances (7α1, 7α2, 7β1, 7β2, and 1-CH_3) are included. δ-meso candidates are labeled a, b, and c. The resonance assigned to the δ-meso is also labeled.

Proximal Histidine Assignments. metGMH4CN exhibits two broad peaks (25.9 and 24.7 ppm) that were barely detected in normal 1D absorption spectra (Figure 2B,C). These peaks became more apparent in the SUPERWEFT spectrum (Figure 2D). These resonances relax extremely fast with apparent nonselective spin–lattice relaxation times, T_1^{app}, of 4.3 ms, as estimated from inversion recovery data. On the basis of their short T_1^{app} and their extreme broadness (T_2 = 0.3 ms), we conclude that these two protons are situated very close to the heme ferric ion. Therefore, we assign the larger resonance to the proximal histidine (His90) C5H imidazole ring proton in the major form of metGMH4CN. This assignment also relies on similar assignments made in model heme complexes and other heme proteins (La Mar & Walker, 1979; Walker & Simonis, 1993). This suggests that the smaller neighbor peak must be due to the same proton in the minor protein form (H90C5H′).

The remaining unassigned proximal histidine proton resonances include the peptide N_pH, CHα, CHβ1, CHβ2, and the ring NπH. A comparison of experiments run in 99.9% D_2O buffer (Figure 8A) and in 90% H_2O/10% D_2O buffer (Figure 8B) allowed complete assignment of these protons, as follows.

In a freshly made sample in 99.9% D_2O buffer, a mutually coupled four-proton spin system (12.64, 11.67, 7.14, and 8.59 ppm at 15 °C, Table 1) was obvious in both COSY and NOESY spectra (Figures 3 and 4). On the basis of assignments made in other low-spin ferriheme proteins (de Ropp et al., 1991a,b; Yamamoto et al., 1991; Satterlee & Erman, 1991; Satterlee et al., 1991; Emerson & La Mar, 1990a,b; Yu et al., 1990), this spin system can be confidently assigned to the N_pH, CαH, and CβH's of the proximal histidine (His90). Typically, in low-spin ferriheme proteins at least one of the proximal histidine's Cβ protons resonates in the high-frequency hyperfine shift region, which led to initial assignment of the single-proton high-frequency resonance (11.67 ppm) as His90 Hβ1. Its most intense cross peak corresponds to its geminal partner Hβ2 (7.14 ppm), with the other cross peak (8.59 ppm) arising from the His90 Hα. The CαH is also weakly coupled to the β2-proton, which suggests that this proton is closer to a cis-dihedral orientation with respect to β2H. In freshly made samples in D_2O, or in samples made up in H_2O, the 12.64 ppm resonance exhibits its full

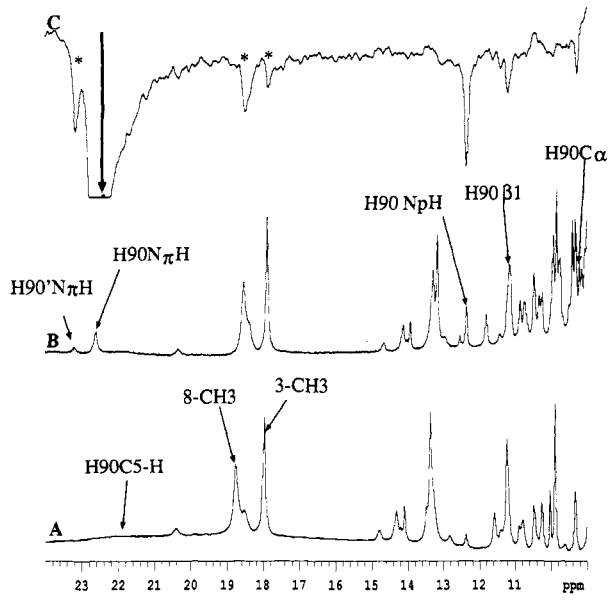

FIGURE 8: Proton hyperfine-shifted portions of the 500-MHz NMR spectra of GMH4CN: (A) in ^2H_2O (pH' 6.42) at 25 °C; (B) in 90% ^1H_2O (pH 6.82) at 25 °C with the His90 spin system labeled; (C) pre-steady-state NOE difference upon irradiation of the H90Nπ H exchangeable peak (large vertical arrow) in 90% ^1H_2O at 25 °C with decoupler spillover indicated by *.

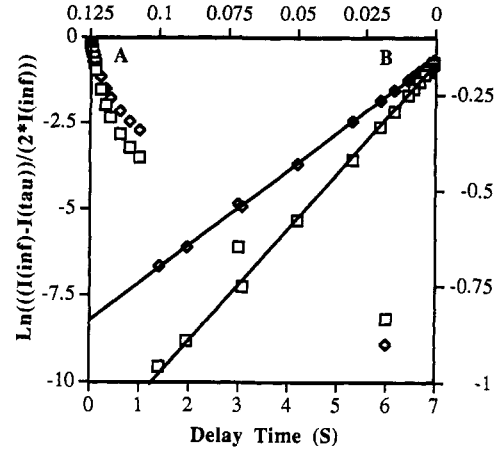

FIGURE 9: Semilog$_e$ plots of inversion–recovery T_1 data for the 8-methyl and 3-methyl resonances: (A) ln (fractional recovered intensity) versus delay time (τ) in seconds for all data out to 6 s (left and bottom coordinates); (B) the initial linear portions over the first 100 ms of relaxation of both sets of data from A (right and top coordinates). It is this linear region from which T_1^{app} is derived.

intensity. However, in D_2O this peak loses intensity over time due to slow isotopic exchange. All of this is consistent with assignment of the 12.64 ppm resonance to the peptide NH (N_pH).

It is interesting to note that COSY data sets produced at extremely fast repetition rates (10–15 s^{-1}) revealed a second set of His90 cross peaks appearing at slightly higher frequencies. The temperature dependence of the less intense set precisely mimics that of the predominant set (Tables 1 and 2). The most logical assignment of this lower intensity set of resonances is to the His90 spin system in the minor metGMH4CN form. This suggests that, in the minor form heme isomer, the proximal histidine's orientation changes minimally.

The remaining proton to be assigned was the ring Nπ H which, on the basis of experience with other low-spin ferriheme protons, should occur near 20 ppm (Satterlee, 1986). Since this proton is typically quite labile to deuterium exchange, it was possible to locate it in 90% H_2O/10% D_2O buffer solutions. Figure 8A shows the downfield portion of the hyperfine-shifted resonances in D_2O, while Figure 8B is an identically acquired spectrum in a 90% H_2O buffer. A new resonance at 22.8 ppm is found in Figure 8B and is assigned to the H90Nπ H proton on the basis of 1D NOE difference experiments. Figure 8C presents the pre-steady-state 1D NOE difference spectrum at 30 °C, produced by saturating the exchangeable resonance at 22.8 ppm for 60 ms. This spectrum shows clear dipolar connectivities to the previously assigned N_pH, Cα H, and Cβ1H protons of His90. The NOE pattern also suggests that this ring proton is oriented toward the peptide NH and is near both Cα H and Cβ1H. The smaller exchangeable peak seen at 23.2 ppm in Figure 8B most likely arises from the Nπ H in the minor isomer. Shift values at 15 °C are reported in Tables 1 and 2.

At this point, a self-consistent set of heme proton assignments for the major protein form of metGMH4CN had been obtained, with only the heme 1-CH_3 and δ-meso assignments still somewhat uncertain (Table 1). The most obvious assignments for the minor form of metGMH4CN that emerged as peripheral information from these experiments are shown in Table 2. Some additional properties of these heme hyperfine-shifted resonances were also studied.

Temperature Dependence of Heme Hyperfine Resonances. The variable-temperature data used for assignments were also collected to determine whether metGMH4CN exhibits any unusual dynamic processes or metal-based electronic structure equilibria that would manifest themselves in non-Curie behavior (La Mar & Walker, 1979; Satterlee, 1986, 1990). In the absence of unusual dynamic processes and equilibria, Curie plots are expected to be linear with extrapolated shift intercepts at $(1/T) = 0$ falling into the diamagnetic chemical shift range, ca. −1 to 10 ppm (Table 1). Linear behavior was found for all of the resonances for which data could be obtained. These data were gathered either directly from 1D spectra, such as for the heme 8-CH_3 and 4-Hα resonances, or indirectly using NOESY and COSY cross peaks (indicated by parentheses in Table 1). Although no anti-Curie temperature dependencies were found, and most of the resonances exhibit extrapolated intercepts in the diamagnetic region, several heme resonances displayed extrapolated Curie intercepts outside the expected range. It is not clear why this occurs, although the error associated with extrapolating a line determined by six data points, taken over a 35-deg temperature range, to an intercept at $(1/T) = 0$ (i.e., T = infinity) is large. However, it may well be that these Curie intercepts are real and characteristic of this protein, since comparable ranges in hyperfine resonance Curie intercepts have recently been reported for a number of peroxidases (Banci et al., 1992).

Spin–Lattice Relaxation Times. Proton spin–lattice relaxation times were measured nonselectively at 500 MHz using the standard 180°–τ–90° pulse sequence. Many of the hyperfine-shifted proton resonances overlap each other, so that accurate values of T_1 could not be determined for all of the hyperfine-shifted resonances. However, for those well-resolved resonances, including resolved exchangeable protons (vide infra), the inversion–recovery intensity data were processed using semilog$_e$ graphs, as previously described (Satterlee, 1986; Satterlee & Erman, 1991; La Mar & de Ropp, 1993). Examples of this data are shown in Figure 9, which are plotted only out to τ = 6.0 s. As indicated by the later time points in Figure 9A, the data appeared nonlinear when viewed over the entire time course of the experiment (τ_{max} = 10 s). This means that throughout the entire time

Table 3: Predicted Fe–Proton Distances for Exchangeable and Nonexchangeable Resonances Based on Relative Relaxation Times

	X-ray data			spin–lattice relaxation	
assignment	F^a	r(Hi) (Å)[b]	r(Hi)/ r(3-CH_3)[c]	(T_1(Hi)/ T_1(3-CH_3))$^{1/6}$ [d]	predicted r(Hi)[e]
3-CH_3	0.99	6.13	1	1	6.13
8-CH_3		6.04	0.985	0.933	5.72
2βc		7.75	1.126	1.149	7.04
2βt		6.80	1.109	1.090	6.68
4α		5.80	0.946	0.953	5.84
4βc		7.68	1.252	1.142	7.00
6α1		5.74			
6α2		6.36	1.037	1.087	6.68
7β1		7.01			
7β2		6.78	1.106	1.066	6.53
His90β2		5.98	0.976	0.961	5.89
His90β1		6.36			
His90 NpH	0.98	7.19	1.17	0.996	6.11[f]
His90 C5H		3.37	0.549	0.532	3.26
His90 NπH	0.98	5.16	0.842	0.769	4.72[f]

[a] Saturation factor (Krishna et al., 1979). [b] Distances derived from the CO crystal structure of the monomer hemoglobin (Arents & Love, 1989, 1991). [c] Ratio of Fe^{2+}–proton distances to Fe^{2+}–3-CH_3 distance. [d] Sixth root of T_1 ratios from Table 1. [e] Predicted Fe^{2+}–proton distances from the spin–lattice relaxation model (Swift, 1973). [f] Predicted Fe^{2+}–proton distances based on 3-CH_3 T_1 (152 ms) measured in a 90% H_2O buffered sample.

regime of the experiment the spin–lattice relaxation for these resonances was not characterized by a single-exponential relaxation process (La Mar & de Ropp, 1993). However, examination of the relaxation data over initial (i.e., short) delay time points revealed linear behavior up to approximately τ = 100 ms (Figure 9B). A single time constant thus characterizes nonselective proton relaxation during the short delay time regime. These time constants are reported in Table 1 as T_1^{app}, the apparent spin–lattice relaxation time that governs the initial relaxation rate.

This type of T_1 analysis, adopted earlier (Satterlee & Erman, 1991), was used in GMH4CN to provide relative estimates of the initial relaxation rates (i.e., T_1^{-1}) for hyperfine-shifted protons. Similar time constants were previously used to estimate iron ion–proton distances for assignment purposes in the metSWMbCN (Cutnell et al., 1980). In paramagnetic molecules such as these, where the proton spin–lattice times are dominated by the paramagnetic contribution (Swift, 1973; La Mar & de Ropp, 1993) to the spin–lattice relaxation rate, T_1^{-1} is given as

$$T_{1i}^{-1} = Dr_i^{-6}f(\tau) + C(A/\hbar)^2 f'(\tau')$$

where the D and C terms represent dipolar and scalar relaxation due to the unpaired spins of the heme iron ion, respectively. In the case where $(A/\hbar)$ is small compared to the first term in the above equation, the ratio of T_1's for two distinct protons in the same molecule is given by

$$T_{1i}/T_{1j} = r_i^6/r_j^6$$

Using this model, along with the T_1^{app} and the Fe^{3+}–proton distance of the 3-methyl as reference data (Arents & Love, 1989), estimates of Fe^{3+}–proton distances for other assigned heme protons could be derived from their measured T_1^{app}'s (Tables 1 and 2). The distances estimated using this method agreed very well with the crystallographically determined distances (Table 3) and provided further support for our set of proton assignments. The relative ordering of the distances for the protons of the heme substituent were virtually identical in both cases:

structure: $2\beta c \approx 4\beta c > 7\beta 1 > 2\beta t \approx 7\beta 2 > 6\alpha 2 > 3 \approx 8 > 4\alpha \approx 6\alpha 1$

relaxation: $2\beta c \approx 4\beta c > 2\beta t = 6\alpha 2 > 7\beta 2 > 3 > 4\alpha \approx 8$

The discrepancies seen between the 8-CH3 and 4α, along with the 6α2 and 7β2, could be explained by different orientations of the vinyl and propionate substituents in solution compared to the crystal structure.

In the same manner, the Fe^{3+}–proton distances estimated by this model for the coordinated proximal His90, including exchangeable protons, agree well with the previously determined distances (Arents & Love, 1989). The relative ordering of the distances was the same:

structure: $N_pH > \beta 1H > N\pi H > C5H$

relaxation: $N_pH > \beta 1H > N\pi H > C5H$

Summary. Homonuclear proton 1D and 2D NMR spectroscopy has been used successfully to assign the heme and proximal histidine protons for metGMH4CN, a myoglobin-like protein. This protein provides a significant test of unorthodox applications of NMR methods (de Ropp et al., 1991a; La Mar & de Ropp, 1993), because the total proton shift dispersion is only 67% that of SWMbCN. The need for making these assignments arises for two reasons: (1) to initiate complete proton assignments for the unusual metGMH4CN heme pocket (Alam et al., 1994; Arents & Love, 1989); and (2) because the hyperfine shift pattern can act as an initial analytical assay for the structural integrity of the heme site in related expressed proteins. An example of this latter problem is shown in Figure 2E, which presents the high-frequency proton hyperfine shift region for a recently expressed mutant of GMH4 (S. L. Alam and J. D. Satterlee, unpublished data). It is obvious from comparing the spectra in Figure 2B-E that the expressed protein has a substantially different hyperfine shift pattern, thereby indicating a different heme ligand binding site. Understanding the structural and/or dynamic differences in the active sites of recombinant GMH4 proteins minimally requires a comprehensive set of heme hyperfine resonance assignments for the wild-type protein. For example, on basis of the assignments presented here (Tables 1 and 2), it can be concluded that the mutant protein represented by the spectrum in Figure 2E contains a much higher percentage of heme inserted within the protein with an orientation identical to that found in SWMbCN.

SUPPLEMENTARY MATERIAL AVAILABLE

Figure containing all additional NOE buildup curves for the 8-methyl resonance (1 page). Ordering information is given on any current masthead page.

REFERENCES

Alam, S. L., Satterlee, J. D., & Edmonds, G. G. (1994) *J. Protein Chem. 13*, 151–164.
Allocatelli, C. T., Cutruzzola, F., Branaccio, A., Brunori, M., Qin, J., & La Mar, G. N. (1993) *Biochemistry 32*, 6041–6049.
Arents, G., & Love, W. E. (1989) *J. Mol. Biol. 210*, 149–161.
Arents, G., & Love, W. E. (1991) Protein Data Bank, Brookhaven National Laboratory.
Aue, W. P., Bartholdi, E., & Ernst, R. R. (1976) *J. Chem. Phys. 64*, 2229–2246.
Banci, L., Bertini, I., Pease, E. A., Tien, M., & Turano, P. (1992) *Biochemistry 31*, 10009–10017.

Bernstein, F. C., Koetzle, T. F., Williams, G. J. B., Meyer, E. F., Jr., Brice, M. D., Rodgers, J. R., Kennard, O., Shimanouchi, T., & Tasumi, M. (1977) *J. Mol. Biol. 112,* 535–542.
Constantinidis, I., & Satterlee, J. D. (1987) *Biochemistry 26,* 7779–7786.
Constantinidis, I., Satterlee, J. D., Pandey, R. K., Leung, H.-K., & Smith, K. M. (1988) *Biochemistry 27,* 3069–3076.
Constantinidis, I. C., Kandler, R. L., & Satterlee, J. D. (1989). *Comp. Biochem. Physiol. 92B,* 619–622.
Cooke, R. M., & Wright, P. E. (1985a) *Biochim. Biophys. Acta 832,* 357–364.
Cooke, R. M., & Wright, P. E. (1985b) *FEBS Lett. 187,* 219–223.
Cooke, R. M., Dalvit, C., Narula, S. S., & Wright, P. E. (1987) *Eur. J. Biochem. 166,* 399–408.
Cutnell, J. D., La Mar, G. N., & Kong, S. B. (1981) *J. Am. Chem. Soc. 103,* 3567–3572.
de Ropp, J. S., Yu, L. P., & La Mar, G. N. (1991a) *J. Biomol. NMR 1,* 175–190.
de Ropp, J. S., Yu, L. P., La Mar, G. N., Wariishi, H., & Gold, M. H. (1991b) *J. Biol. Chem. 226,* 5001–5008.
Emerson, S. D., & La Mar, G. N. (1990a) *Biochemistry 29,* 1545–1556.
Emerson, S. D., & La Mar, G. N. (1990b) *Biochemistry 29,* 1556–1566.
Ernst, R. R., Bodenhausen, G., & Wokaun, A. (1986) in *Principles of Nuclear Magnetic Resonance in One and Two Dimensions,* Clarendon Press, Oxford, UK.
Granot, J. (1982) *J. Magn. Reson. 49,* 257–270.
Harris, R. K. (1983) in *Nuclear Magnetic Resonance Spectroscopy: A Physiochemical View,* Pitman Publishing Inc., Marshfield, MA.
Hore, P. J. (1983) *J. Magn. Reson. 55,* 283–300.
Imamura, T., Baldwin, T. O., & Riggs, A. H. (1972) *J. Biol. Chem. 247,* 2785–2797.
Inubushi, T., & Becker, E. D. (1983) *J. Magn. Reson. 51,* 128.
Jue, T., Krishnamoorthi, R., & La Mar, G. N. (1983) *J. Am. Chem. Soc. 105,* 5101–5103.
Kandler, R. L., & Satterlee, J. D. (1983) *Comp. Biochem. Physiol. 75b,* 499–503.
Kandler, R. L., Constantinidis, I., & Satterlee, J. D. (1984) *Biochem. J. 226,* 131–138.
Keller, R. M., & Wuthrich, K. (1981) in *Biological Magnetic Resonance* (Berliner, L. J., & Reuben, J., Eds.) Vol. 3, pp 1–52, Plenum Press, New York.
Kumar, A., Wagner, G., Ernst, R. R., & Wuthrich, K. (1981) *J. Am. Chem. Soc. 103,* 3654–3658.
Kuriyan, J., Witz, S., Karplus, M., & Petsko, G. A. (1986) *J. Mol. Biol. 192,* 133–154.
La Mar G. N., & Walker, F. A. (1979) in *The Porphyrins* (Dolphin, D., Ed.) Vol. IV, pp 61–157, Academic Press, New York.
La Mar, G. N., & de Ropp, J. S. (1993) in *Biological Magnetic Resonance* (Berliner, L. J., & Reuben, J., Eds.) Vol. 12, pp 1–78, Plenum Press, New York.
La Mar, G. N., de Ropp, J., Chacko, V. P., Satterlee, J. D., & Erman, J. E. (1982) *Biochim. Biophys. Acta 708,* 317–325.
Lecomte, J. T. J., & La Mar, G. N. (1987) *J. Am. Chem. Soc. 109,* 7219–7220.
Li, S. L., & Riggs, A. F. (1971) *Biochim. Biophys. Acta 236,* 208–210.
Macura, S., Huang, Y., & Suter, D. (1981) *J. Magn. Reson. 43,* 259–281.
Mintorovitch, J., & Satterlee, J. D. (1988) *Biochemistry 27,* 8045–8050.
Mintorovitch, J., van Pelt, D., & Satterlee, J. D. (1989) *Biochemistry 28,* 6099–6104.
Mintorovitch, J., Satterlee, J. D., Pandey, R., Lewis, H., & Smith, K. M. (1990) *Inorg. Chim. Acta 170,* 157–159.
Moss, G. P. (1988) *Eur. J. Biochem. 178,* 277–328.
Neuhaus, D., & Wiliamson, M. (1989) in *The Nuclear Overhauser Effect in Structural and Conformational Analysis,* VCH Publishing, New York.
Padlan, E., & Love, W. E. (1974). *J. Biol. Chem. 249,* 4067–4078.
Parkhurst, L. J., Sima, P., & Goss, D. J. (1980) *Biochemistry 19,* 2688–2692.
Peyton, D. H., La Mar, G. N., Pande, U., Ascoli, F., Smith, K. M., Pandey, R. K., Parish, D. W., Bolognesi, M., & Brunori, M. (1989) *Biochemistry 28,* 4880–4887.
Qin, J., La Mar, G. N., Ascoli, F., Bolognesi, M., & Brunori, M. (1992) *J. Mol. Biol. 224,* 891-897.
Qin, J., La Mar, G. N., Cutruzzola, F., Allocatelli, C. T., Brancaccio, A., & Brunori, M. (1993) private communication.
Rajarathnam, K., La Mar, G. N., Chiu, M., & Sligar, S. G. (1992) *J. Am. Chem. Soc. 114,* 9048–9058.
Satterlee, J. D. (1984) *Biochim. Biophys. Acta 791,* 384–394.
Satterlee, J. D. (1985) *Annu. Rept. NMR Spectrosc. 17,* 79–178.
Satterlee, J. D. (1990a) *Concepts Magn. Reson. 2,* 69–79.
Satterlee, J. D. (1990b) *Concepts Magn. Reson. 2,* 119–129.
Satterlee, J. D., & Erman, J. E. (1991) *Biochemistry 30,* 4398–4405.
Satterlee, J. D., Erman, J. E., & de Ropp, J. S. (1987) *J. Biol. Chem. 262,* 11578–11583.
Satterlee, J. D., Russell, D. J., & Erman, J. E. (1991) *Biochemistry 30,* 9072–9077.
Satterlee, J. D., Alam, S., Yi, Q., Erman, J. E., Constantinidis, I., Russell, D. J., & Moench, S. J. (1993) in *Biological Magnetic Resonance* (Berliner, L. J., & Reuben, J., Eds.) Vol. 12, pp 275–298, Plenum Press, New York.
Simons, P. C., & Satterlee, J. D. (1989) *Biochemistry 28,* 8525–8530.
Simons, P. C., & Satterlee, J. D. (1990) in *Structure and Function of Invertebrate Oxygen Carriers* (Vinogradov, S. H., & Kapp, O. H., Eds.) pp 171–177, Springer-Verlag, New York.
States, D. J., Haberkorn, R. A., & Ruben, D. J. (1982) *J. Magn. Reson. 48,* 286–292.
Swift, T. J. (1973) in *NMR of Paramagnetic Molecules* (La Mar, G. N., Horrocks, W. D., Jr., & Holm, R. H., Eds.) pp 55–83, Academic Press, New York.
Walker, F. A., & Simonis, U. (1993) in *Biological Magnetic Resonance* (Berliner, L. J., & Reuben, J., Eds.) Vol. 12, pp 133–274, Plenum Press, New York.
Wuthrich, K. (1986) *NMR of Proteins and Nucleic Acids,* Wiley-Interscience, New York.
Xia, Z. X., & Mathews, F. S. (1990) *J. Mol. Biol. 212,* 837–863.
Yamamoto, Y., & Suzuki, T. (1993) *Biochim. Biophys. Acta 1163,* 287–296.
Yamamoto, Y., Osawa, A., Inoue, Y., Chujo, R., & Suzuki, T. (1989) *FEBS Lett. 247,* 263–267.
Yamamoto, Y., Iwafune, K., Nanai, N., Osawa, A., Chujo, R., & Susuki, T. (1991) *Eur. J. Biochem. 198,* 299–306.
Yip, P. F. (1990) *J. Magn. Reson. 90,* 382–383.
Yu, L. P., La Mar, G. N., & Rajarathnam (1990) *J. Am. Chem. Soc. 112,* 9527–9534.